Journal of African Earth Sciences xxx (xxxx) xxx

Contents lists available at ScienceDirect

Journal of African Earth Sciences

journal homepage: www.elsevier.com/locate/jafrearsci

Genesis and paleoenvironmental analysis of the ironstone facies of the Maastrichtian Patti Formation, Bida Basin, Nigeria

O.J. Ojo [a,*], T.E. Bamidele [b], S.A. Adepoju [b], S.O. Akande [c]

[a] Department of Geology, Federal University Oye-Ekiti, Nigeria
[b] Department of Geology and Mineral Sciences, Kwara State University, Malete, Nigeria
[c] Department of Geology and Mineral Sciences, University of Ilorin, Nigeria

ARTICLE INFO

Keywords:
Ahoko
Diagenesis
Kaolinite
Anoxic
Transgression

ABSTRACT

The recently constructed Lokoja-Abuja highway and a quarry which cut through the Patti Formation, provided opportunity for the field study and sampling of the exposed ironstone interbeds within the carbonaceous shales and clays in Ahoko-Idu axis of the southern Bida Basin, Nigeria. The origin and paleoenvironmental significance of the ferruginous intervals were examined in this paper. Investigation reveals that the ferruginous bands occur as three lithofacies comprising of laminated, bioturbated and spheroidal concretionary facies. The primary components and depositional features of the host shales (detrital minerals, wood and herbaceous fragments, laminations) are largely preserved in the ironstones indicating compositional similarity and therefore a diagenetic origin for the ironstones. Results of XRD reveal substantial amount of siderite and illite but minor amounts of kaolinite, hematite, calcite and magnetite. Major elements such as Fe_2O_3, SiO_2, Al_2O_3, CaO, MgO and P_2O_5 range from 41.50 to 54.60%, 6.10–23.30%, 3.64–7.00%, 1.40–13.60%, 0.30–1.20% and 0.10–8.80% respectively. The current data is suggestive that kaolinite was diagenetically replaced by siderite at early stage of burial in a reducing environment. Migrating pore water, probably enriched with alkali metals like Ca and Mg, sourced from sea water in the depositional basin and abundance of organic matter in the primary sediments are interpreted to be part of the factors responsible for the siderite precipitation. Both the host shale and the ferruginous beds contain significant amount of MgO, CaO, relics of dissolved bioclasts and body fossils. The geochemical proxies combined with the presence of magnesian siderite in the ironstones indicate that the host shales were deposited in marine environment with occasional freshwater influence. The study concludes that the ironstones are marine to non-marine, sideritic and diagenetic. The laminated and fossiliferous ironstone facies was deposited at the peak of marine transgression during the Upper Cretaceous time and represents maximum flooding surface. Shallowing up and regression into fresh water swamp condition was marked by the occurrence of freshwater sideritic ironstone.

1. Introduction

The Earth crust is substantially enriched with iron and is present in various concentration levels in most rocks. Discussions on the origin of iron bearing sediments, that is much richer in iron minerals than usual have been of interest and received attention among researchers (Loope et al., 2012; Afify et al., 2018; Akinlotan, 2019). In a number of previous studies, geochemical proxies and compositional features of outcropping ironstone beds have been used for the interpretation of the paleoenvironments of sedimentary successions in a basin. Examples include the work of Choi et al. (2003) on the siderites from Holocene coastal deposits of Korea and that of Curtis et al. (1975) which examined the origin of the concretional siderites in the Westphalian of Yorkshire. Akande and Mücke (1993) reconstructed the depositional processes from the sideritic carbonate sediments at Leru in Anambra Basin, Nigeria.

In this present paper, investigation on the ironstones facies of the Maastrichtian Patti Formation in the Bida Basin, Nigeria is reported. The current study area is situated between Idu and Ahoko axis (Fig. 1) along the Lokoja-Abuja highway where excellent sections of the shale-clay member of the Patti Formation are exposed.The Bida Basin is an oval shaped intracratonic sedimentary feature, elongated along northwest-

* Corresponding author.
E-mail address: olusola.ojo@fuoye.edu.ng (O.J. Ojo).

https://doi.org/10.1016/j.jafrearsci.2020.104058
Received 22 May 2020; Received in revised form 24 October 2020; Accepted 26 October 2020
Available online 27 October 2020
1464-343X/© 2020 Elsevier Ltd. All rights reserved.

southeast direction and perpendicular to the main axis of the Benue Trough (Fig. 1). It is a rift related basin associated with Early Cretaceous separation of southern America plate from the African plates. The basin is filled with flat lying clastic sediments of about 3.5 km thick (Udensi and Osazuwa, 2004). It is contiguous to the Anambra Basin in the southeast while to the northwest it is adjacent to Sokoto Basin. These basins were depocenters for transgressive and regressive sediments during Late Cretaceous period in Nigeria. The Bida Basin is widely believed to be an area of local subsidence formed during the Campanian-Maastrichtian age, during which the South Atlantic–Tethys seaway was probably routed through the basin (Kogbe, 1976; Ojo and Ajakaiye, 1989; Mücke, 2000).

The stratigraphy of Bida Basin as presented by Jones (1958) and Adeleye (1973) consists of the Campanian Lokoja Formation which is predominantly of sandstones and it overlies non-conformably the crystalline basement rocks in the southern Bida Basin. The Maastrichtian Patti Formation (made up of sandstone, shale, ironstone and claystone) overlies the Lokoja Formation. Ojo and Akande (2009) identified and described two distinct members of this formation as Shale-clay member (comprising of well bedded shale, ironstone and claystone deposited predominantly in relatively quiet shallow marine environment) and the sandstone member deposited in neashore to shoreface environments. According to Ojo and Akande (2006), the typical lithological characteristics (predominance of clay sized sediments, laminations, bioturbations) of the shale-clay member of the Patti Formation indicate low energy, quiet setting ranging from fresh water to nearshore marine swamps. The fossiliferous shales and the ferruginised facies which contain marine mollusk shells and Ophiomorha burrows at the lower part of the sequence suggest marine incursion. The overlying siltstones (containing large woody fragments), coaly shales, lignites and kaolinitic claystones indicate development of freshwater proximal deltaic plain and floodplain. These processes provide indication of fluctuation of the local coastline typical of the Nigeria Maastrichtian sedimentation history. The Agbaja Formation (ironstone) probably of Late Maastrichtian rests on the two older formations and is made up of oolitic and pisolitic ironstones. To the northern part of the basin, the previously described

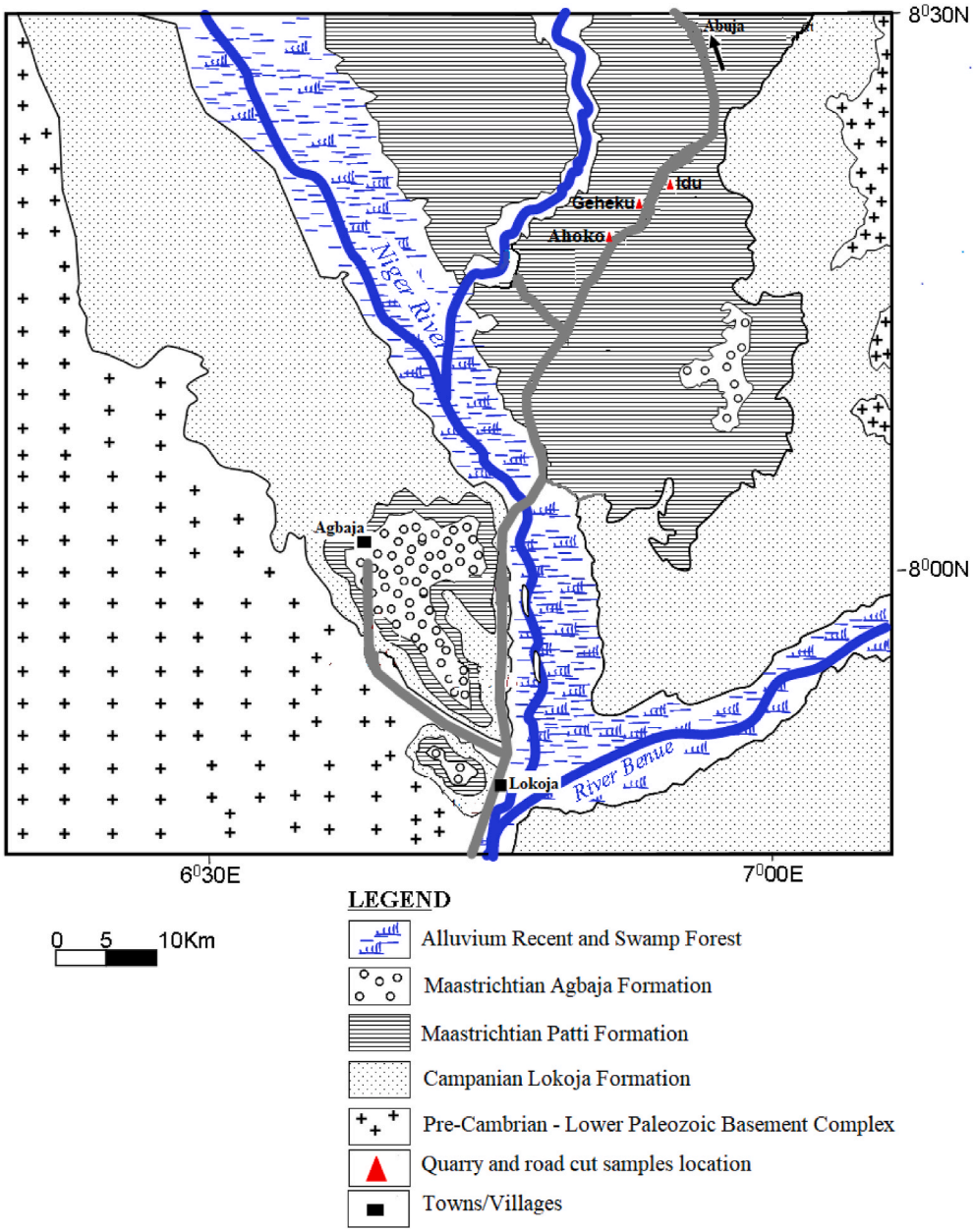


Fig. 1. Geological map of Nigerian and location of the study area.

rock units can be correlated with the Bida Formation, Sakpe Ironstone, Enagi Formation, and Batati Ironstone (Fig. 2).

In spite of the genetic significance of this well bedded and prominent iron bearing units with potential implications for understanding the Late Cretaceous paleogeography of the basin, they remained uninvestigated. Aspects such as facies analysis, petrography, mineral paragenesis and geochemical characteristics of Agbaja Ironstone which have been studied and published (Ladipo et al., 1994; Abimbola et al., 1999; Mücke, 2000) have not been undertaken for the Patti Formation ironstone in Ahoko, Geheku and Idu areas of the southern Bida Basin. Therefore, the ironstones were evaluated in this study, for the first time, with the following objectives; (i) investigate the lithofacies of the ironstones (ii) evaluate their petrographic and mineralogical composition (iii) determine the geochemical composition and (iv) use the above information to interpret the origin and assess its paleoenvironmental indicator potential within the context of constraining the paleogeography of the basin and its regional implications. The present study is significant because to date, no such work has been carried out on the ironstones and in addition, it serves to compliment previous efforts on the understanding of the paleogeography of the basin.

Hydrocarbon prospecting in a frontier basin like Bida Basin requires an understanding of the depositional environments of the sedimentary succession and realistic prediction of the source rocks strongly depends on accurate reconstruction of the depositional history of the sediments. Ojo and Akande (2006, 2008) provided an insight as regards the influence of shallow marine condition during Maastrichtian sedimentation in the Bida Basin from the point of view of palynological data from the shales. The present study is however designed to give an insight from the ferruginous facies that are interbedded with the shales in the study area. Afify et al. (2015, 2018) and Akinlotan (2019) recently demonstrated the significance of ironstones hosted in clastic sediments as paleoenvironmental indicators.

2. Field work, sampling and analytical methods

The Lokoja-Abuja high way construction and a quarry provides excellent road cuts and quarry face exposure of the argillaceous units and ironstones of the Patti Formation in the study area. Three vertical profiles located at Ahoko (N008°18′14.8″; E006°51′28.0″), Geheku (N008°18′51.8″; E006°52′34.5″) and Idu (N008°19′11.2″; E006°52′46.0″) were logged (Fig. 3). Facies analysis of the ironstone was carried out leading to the establishment of three lithofacies. Samples were selected from the sections at Ahoko, Geheku and Idu and each lithofacies of the ironstone is represented in the selection. Six samples were selected from Ahoko section which is the thickest among the studied sections while three and two samples were selected from Geheku and Idu sections respectively.

For mineralogical studies and petrofacies classification eleven samples were selected and prepared for thin section (about 0.03 mm thickness) slides and viewed under high transmitted light microscope at the Department of Geology and Mineral Sciences, University of Ilorin, Nigeria. The consolidated samples were cut and thereafter mounted on glass slides using Canadian balsam. The mounted samples were grinded on a lap wheel with coarse abrasive, washed and the samples were finally grinded manually with sludge of fine abrasive on a glass plate to the desired thickness which permitted microscopic observation of the petrographic properties of the samples. Photomicrographs of representative field of view were taken and documented. The polish section of the samples were also prepared by cutting slabs of 1 cm × 1 cm ×0.5 cm dimension in the laboratory. After washing, the samples were finally grinded manually with sludge of fine abrasive on a glass plate to the desired surface smoothness which can allow microscopic observation of the internal features of the samples using reflected light microscope. It is to be noted that the pervasive iron replacement on the sediments have impacted on the clarity of some of the photomicrographs presented.

Mineral composition was also obtained from X-Ray Diffraction analysis carried out at the Department of Geology, Faculty of Natural and Agricultural Sciences, University of Pretoria, South Africa. Prior to analysis, seven selected samples of the ironstones were pulverized into finer materials. After the pulverization of the representative samples using a riffle splitter, the samples were loaded in a tungsten carbide vessel and prepared according to the standardized Panalytical backloading system, which provides nearly random distribution of the particles. They were then analyzed using a PANalytical X'Pert Pro powder diffractometer in θ–θ configuration with an X'Celerator detector and variable divergence- and fixed receiving slits with Fe filtered Co-Kα radiation (λ = 1.789 Å). The phases were identified using X'Pert Highscore plus software. The relative phase amounts (weight%) were estimated using the Rietveld method (Autoquan Program) based on the relative peak intensities of the respective minerals in the XRD charts. Errors are on the 3 sigma level.

Nine samples of the ironstones were selected and analyzed for bulk elemental composition; major Oxides, trace Elements (TE) and rare earth elements (REE) using both X-ray Fluorescence (XRF) and Aqua

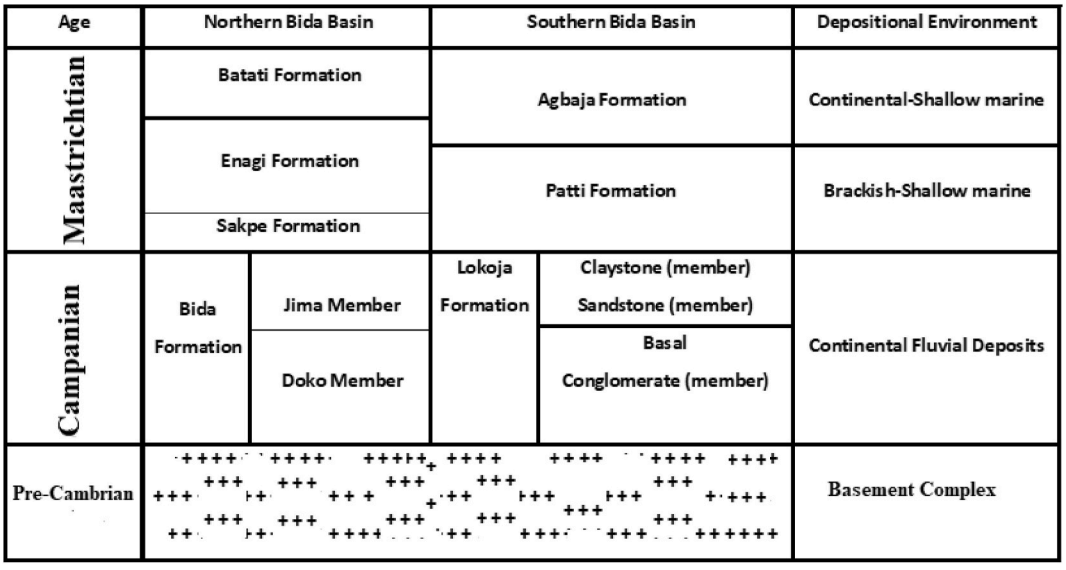


Fig. 2. Regional Stratigraphic setting of the Bida Basin (Modified after Adeleye, 1973).

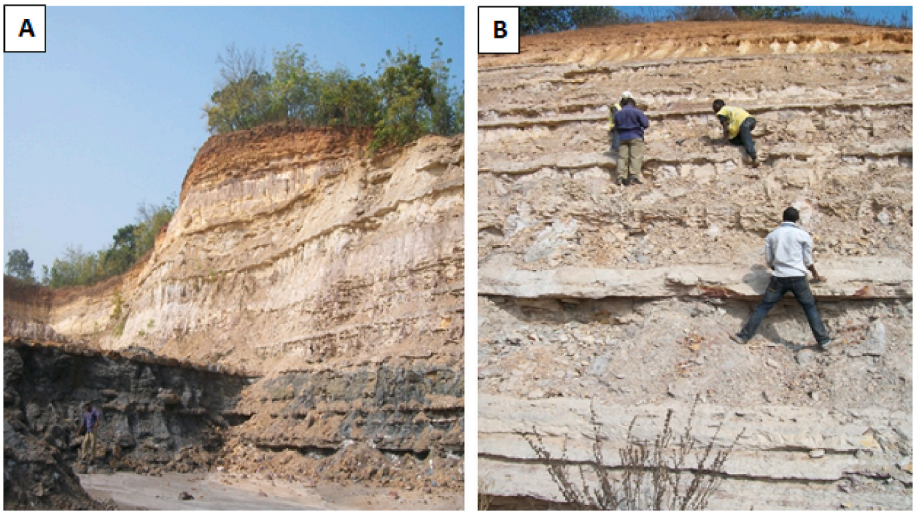


Fig. 3. (a) Quarry face and road cut exposures of the investigated sediments at Ahoko (N008° 18′14.8″E 006°51′28.0″) and (b) at Geheku (N008°18′51.8″E 006°52′34.5″) respectively. Note the height of the man standing upright in Fig. 3a is 1.65m while the one in Fig. 3b is 1.70 m.

regia ultra-trace Inductively Coupled Plasma Mass Spectroscopy (ICP-MS) analyses which were carried out at ACME Analytical Laboratories (Acme Lab), Canada. The samples splits for XRF analysis were pulverized to 85% passing 200mesh (75 μm) in a mild-steel ring-and-puck mill following the dryness at 60 °C followed by pulverization via a jaw crusher to 70% passing a 10 mesh (2 mm). A 0.2 g aliquot was weighed into a graphite crucible and mixed with 1.5 g of $LiBO_2/Li_2B_4O_7$ flux. The crucibles were heated in a 980 °C oven for 30 min. The resulting bead was dissolved in 5% HNO_3 (ACS grade nitric acid diluted in dematerialized water). Samples and calibration reagent blanks were aspirated into an XRF (SpectroCiros Vision or Varian 735) to determine the set of major oxides and elements. Loss on ignition (LOI) was determined by

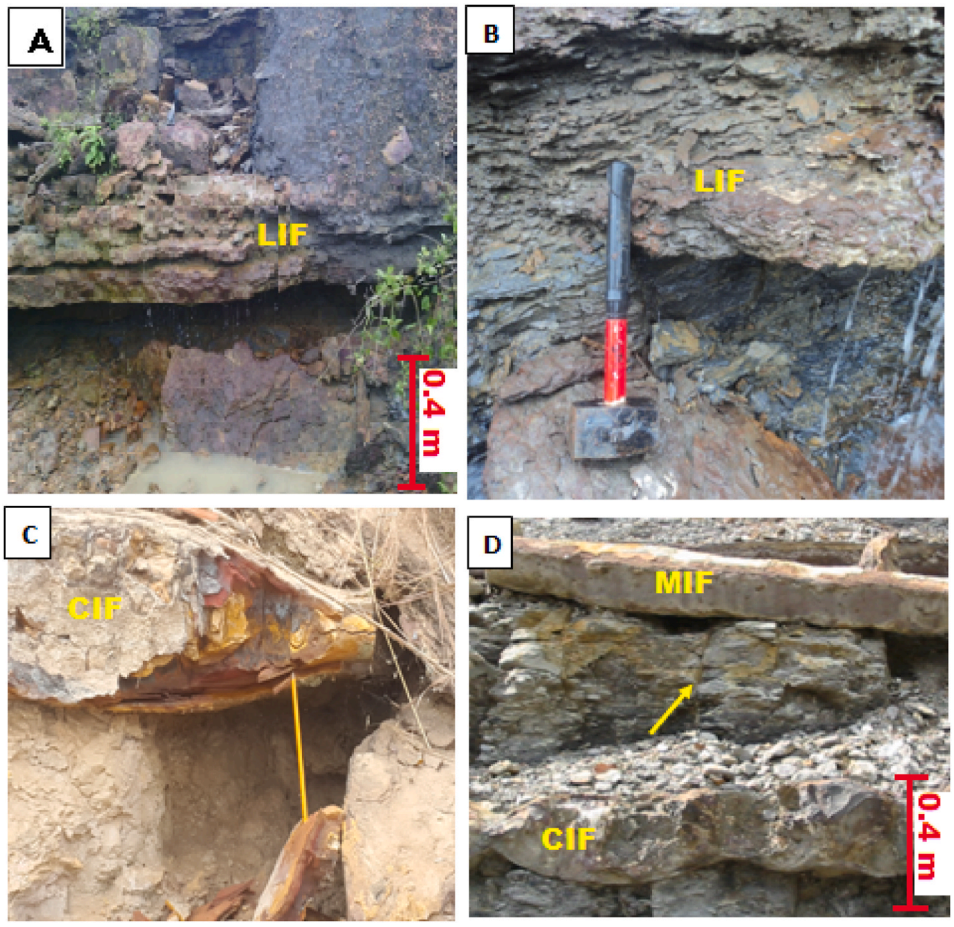


Fig. 4. Field photographs of the ironstone facies interbedded within the shales. A and B: Laminated fossiliferous ironstone lithofacies LIF, C: Spheroidal lithofacies CIF, D: Bioturbated massive lithofacies MIF with *Thalassinoides* burrows.

igniting a 1.0 g sample split at 950 °C for 90 min, then measuring the weight loss. Samples for (ICP-MS) analysis were pulverized to 95% passing 150mesh (100 μm) in a mild-steel ring-and-puck mill. A 0.2 g aliquot was weighed into a graphite crucible and mixed with 1.5 g of $LiBO_2/Li_2B_4O_7$ flux. The crucibles were heated in a 980 °C oven for 30 min. The resulting bead was dissolved in 100 mL 5% HNO_3 (ACS grade nitric acid diluted in demineralized water). An aliquot of the solution was poured into a polypropylene test tube. Samples and calibrated reagent blanks were aspirated into an ICP-MS (PerkinElmer Elan 6000 or 9000) and a digested split of 0.5 g in Aqua Regia aspirated into an ICP-MS to determine the elements.

3. Results

3.1. Field and facies characteristics

Field investigation of exposed part of Maastrichtian Patti Formation around the centre (Idu – Acheni axis) of the southern Bida Basin shows that the ironstones are interbedded with argillaceous rocks (carbonaceous shale, siltstone, claystone and lignite). At these localities (Ahoko, Geheku and Idu) the quarry and road cuts exposed between 15 and 20m thick sections of the sediments. The ironstone frequently occurs as laterally continuous bands, concretions and in some cases as lenses (Figs. 3 and 4). Facies analysis of the ferruginous unit permits recognition of three sub-facies consisting of horizontal laminated and fossiliferous ironstone facies, concretional and spheroidal ironstone facies and bioturbated massive ironstone facies. Field study reveals a striking feature in which the shales contain vertical fractures but the fractures terminate at the base and top of each ironstone bed (that is, do not cut through the ironstones) (Fig. 4D). The fractures in places are filled with ferruginous clastic materials.

3.2. Horizontal laminated ironstone facies

This facies of ironstone is restricted to the lower part of the sections in the study area. They are weakly to distinctly laminated. The laminations are parallel to wavy in places and a typical feature of this facies is their fossiliferous nature. Bivalves, pelecypods and gastropods are preserved in the ironstone in form of body and trace fossils. This unit is about 0.5 m thick (Fig. 4A and B). This facies is associated with well laminated, dark to grayish shales that are rich in organic matter and equally fossiliferous. At Ahoko and Geheku sections, they occur at the lower part.

3.3. Concretional and spheroidal ironstone facies

This facies exhibits concretionary and spheroidal laminations and the concretions are of varying sizes. The small flattened concretions with poorly developed concretional structure are generally less than 0.1 × 0.3 m in dimension while the large ones have an average dimension of 0.35 × 0.7 m (Fig. 4C and D). Close examination of the pisolites shows that some have concretion with unconsolidated core are enclosed by concentric cortex of sideritic bands. The core retains the primarily deposited materials (clay, silt and sand) which are in part diagenetically replaced by iron precipitates. The core of this type of concretion contain preserved primary detrital fine grains of sand, silt and clay. This feature and compositional characteristics presumably reflects selective ferruginization and iron mineral enrichment of the original clastic materials. Other concretions are highly indurated exhibiting well lithified cores enclosed by concentric or roughly concentric cortexes of sideritic lamina.

3.4. Bioturbated ironstone facies

This facies of ironstone lacks internal organization (massive) but is rich in burrows of *thalassinoides* and *ophiomorpha* which are now filled with ferruginized clayey to silty particles (Fig. 4D). The thickness of this ironstone facies in the Ahoko and Geheku sections ranges between 0.2 m and 0.3m. It is unique, infrequent and restricted to the middle part of the section. It is silty and contains a lot of preserved original organic rich shaly materials and woody fragments.

3.5. Petrography and facies characteristics

Detailed thin section microscopic studies coupled with field description of the ironstones were used to characterize the ironstones into three petrofacies. The grain size and fabric were basically used as the lithofacies parameters here and these petrofacies types are presented below:

3.6. Sandy ironstone

The sandy ironstone occurs as a thin laminated to massive bed at the Gehuku and Idu sections. They consist of iron minerals precipitated within intergranular spaces in fine grained sandy matrix. It is grain to matrix supported with some of the quartz grains showing point contact whereas some floats. The fine grained quartz occurs as angular-to sub-rounded grains and show pleichroism in polarized light (Fig. 5A). They are cemented together by admixture of siderite and probably hematite. These components are embedded in the slightly to highly hematitized clay matrix with dark hematite and siderite as cement.

3.7. Silty ironstone

This petrofacies is characterized by silt to fine sand size detrital quartz supported by plant remains and clay (Fig. 5B). The organic materials in places impact some level of greyish colour and commonly exhibit a matrix-supported fabric. Here there is lack of internally organized structure which is likely due to the effect of bioturbation by the scavenging organisms. The matrix and framework grains consequently display concentric or cylindrical iron rich matrix along the burrows (Fig. 6B).

3.8. Clayey ironstone

The clayey ironstone is dominated by a ground mass consisting mainly of admixture of clay minerals such as kaolinite, smectite, chlorite and iron bearing minerals such as siderite, hematite and goethite. This facies is characterized by replacement of the clay precursor (mainly kaolinite) by iron mineral precipitates which are expressed by different level of pigmentation (some slightly pigmented and others highly pigmented). The pigmentation was used as a basis for further classifying the ironstones into the slightly pigmented (Fig. 5C) which are indicative of partial replacement of the clay precursors while the highly pigmented are indicative of the clay precursor which is now totally replaced by iron minerals. In ordinary light, some of the preserved kaolinite display white colour.

3.9. Mineralogy

The X-ray diffraction analysis of the samples reveals the presence of siderite ($FeCO_3$), quartz (SiO_2), hematite (Fe_2O_3), calcite ($CaCO_3$), anatase (TiO_2), illite$\{[K0{\cdot}6(H_3O)_{0.4}]Al_{1.3}Mg0{\cdot}3Fe_2+\ 0.1Si_{3.5}O_{10}(OH)_2{\cdot}(H_2O)\}$, ilmenite, ($FeTiO_2$) and kaolinite ($Al_2Si_2O_5(OH)_4$) (Fig. 7, Table 1). It was observed that illite and siderite dominate the mineral constituents ranging from 20.17 to 29.66% and 0.07–23.94% with average of 26.3% and 15.97% respectively. An exceptionally low quantity (0.07%) of siderite was recorded in the sandy ironstone from Idu. Siderite quantity is higher in the samples from Ahoko than those from Geheku and Idu sections. Very high concentration of SiO_2 was observed in sample JID1A at Idu, and this agrees with the petrographical observations, which show the presence of euhedral quartz in significant amount in the samples (Fig. 5A). Sharp

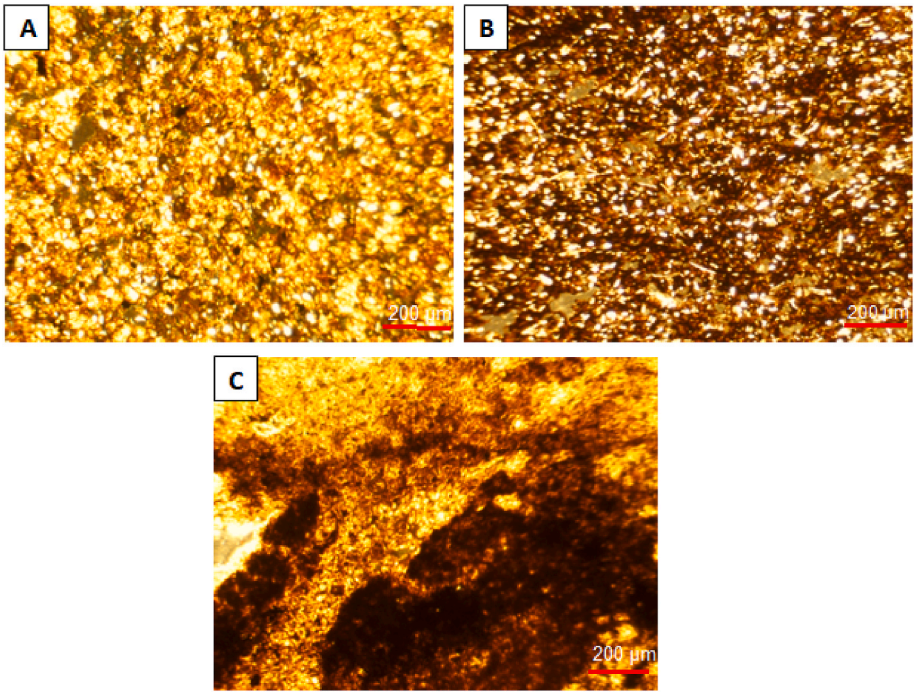


Fig. 5. (A) Sandy Ironstone microfacies. Note the angular to rounded white quartz grains (B) Silty Ironstone. Note the poorly sorted admixture of clay, silt size quartz grains and plant remains (C) Clayey Ironstone, Note dark irregular patches domains within the highly pigmented admixture of siderite and clay groundmass. (Long black arrows - sideritic groundmass, short black arrow - kaolinitic groundmass).

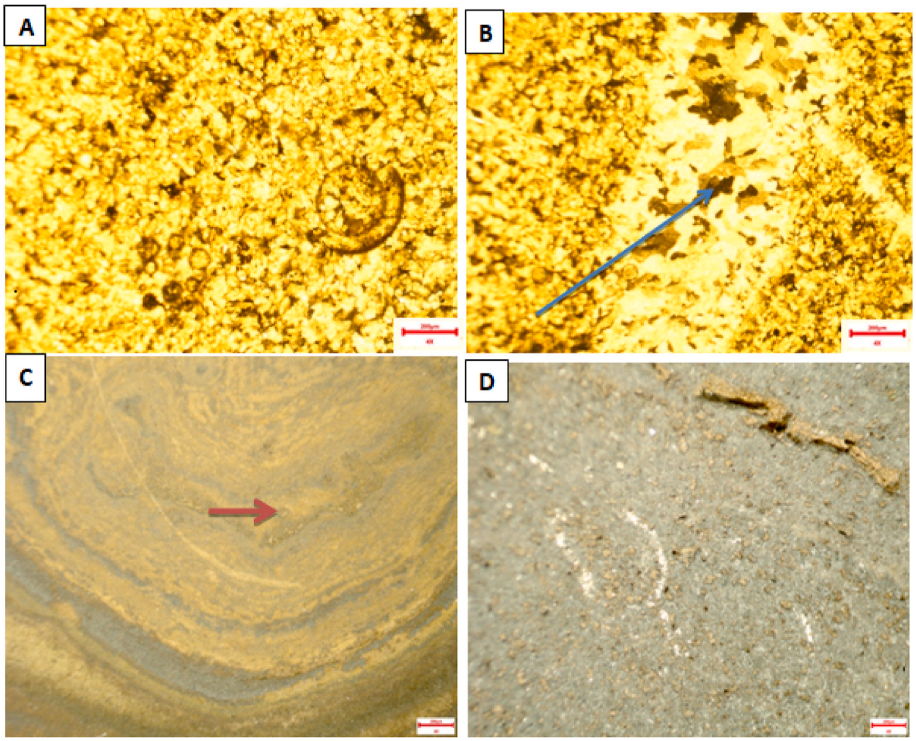


Fig. 6. Photomicrograph showing; (A) Sideritized bivalve shell in the laminated fossiliferous ironstone facies; (B) Bioturbated facies showing recrystallized burrow, (C) Polished section of Spheroidal facies. Note different stages of induration with iron, dark band representing total replacement of the clay precursor. (D) Ferruginized shale with groundmass selectively replaced by siderite precipitates. Note the relics of the gastropod.

peaks of quartz reflect the good crystallinity of this mineral in the Benavi IRS samples (Yasin, 2009).

Kaolinite, hematite, calcite and magnetite occur in all the samples almost in equal amounts. The identification of this mineral was based on its basal reflection d = 1.98A°, other d-spacing for kaolinite includes: 4.44A°, 4.4A° and 2.34 A° (Fig. 7). Kaolinite is a product of chemical weathering involving hydrolysis of feldspars in a warm tropical climate. It is subsequently transported and deposited out of suspension as

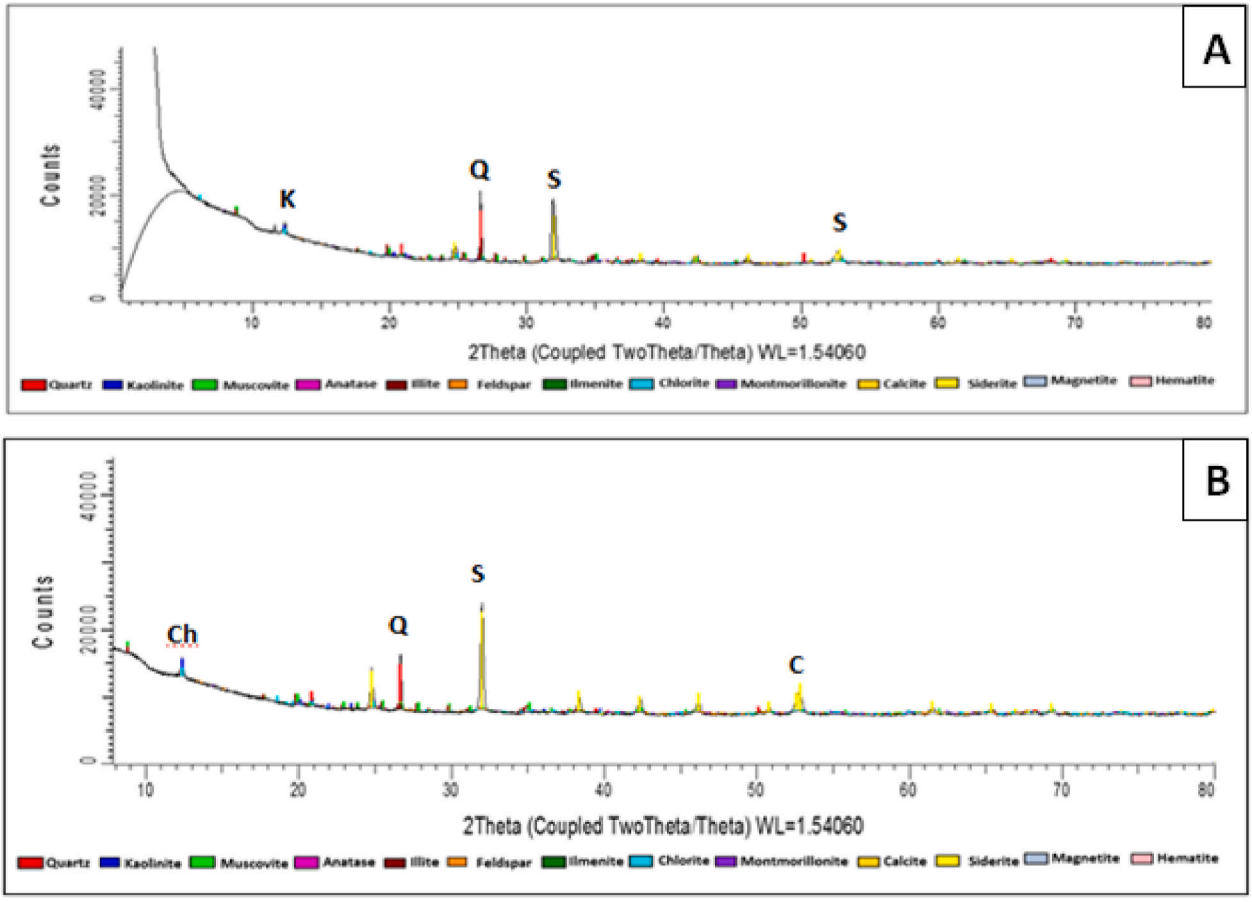


Fig. 7. XRD diffractogram of ironstone samples (a) BGH1E showing peaks for K- kaolinite, S-siderite and Q-quartz and (b): JAH1B showing peaks for Ch-Chlorite, Q-quartz, S-siderite and C-calcite.

Table 1
Mineral constituents of the investigated samples (%).

Mineral	BGH1E	JAH1JA	JAH1B	JAH1JB	JAH1R	JAH1T	JID1A
Quartz	13.14	11.25	9.56	7.45	18.94	12.23	30.17
Kaolinite	8.05	10.03	11.91	10.12	9.78	9.72	2.12
Muscovite	25.90	23.02	24.48	22.57	21.20	21.10	29.48
Anatase	0.20	0.29	0.42	0.33	0.18	0.46	0.00
Illite	29.25	23.69	20.17	24.67	29.70	27.21	29.66
Feldspar	1.55	2.30	1.03	3.24	0.87	2.70	0.57
Ilmenite	0.15	0.35	0.21	0.16	0.22	0.45	0.11
Chlorite	7.29	5.81	8.58	5.39	6.90	3.91	4.47
Montmorillonite	0.10	0.17	0.08	0.02	0.02	0.00	0.00
Calcite	0.27	0.72	0.30	0.24	0.11	1.15	0.18
Siderite	13.37	20.91	22.34	23.94	10.94	20.22	0.07
Magnetite	0.36	0.66	0.75	0.54	0.67	0.46	0.28
Hematite	0.37	0.80	0.18	1.34	0.46	0.17	2.88
Total	100	100	100.01	100.01	99.99	99.78	99.99

Table 2
Major Oxides (%) composition of the investigated ironstone.

Location	Sample	SiO_2	Al_2O_3	Fe_2O_3	CaO	MgO	Na_2O	K_2O	MnO	TiO_2	P_2O_5	LOI
AHOKO	**JAH1B**	13.43	5.29	47.48	1.41	2.49	<0.01	0.25	1.19	0.61	0.24	26.78
	JAH1N	23.68	7.49	41.02	1.64	1.72	<0.01	0.47	0.62	0.88	0.12	20.54
	JAH1R	22.24	6.99	41.68	1.67	1.82	<0.01	0.43	0.63	0.83	0.12	21.58
	JAH1T	10.02	4.51	49.72	2.69	2.60	<0.01	0.22	0.31	0.34	0.34	27.86
	JAH1JA	12.21	5.49	44.25	6.10	1.89	0.04	0.31	0.33	0.45	3.15	23.65
	JAH1JB	8.41	3.84	36.46	13.97	1.84	0.16	0.23	0.32	0.29	8.81	23.08
GEHEKU	**BGH1C**	12.90	3.97	49.61	2.90	2.33	<0.01	0.34	0.43	0.47	0.78	25.36
	BGH1E	17.11	5.48	45.64	2.26	2.84	<0.01	0.42	0.30	0.68	0.13	23.81
IDU	**JID1A**	52.50	1.79	40.47	0.08	0.05	<0.01	0.10	<0.01	0.67	0.04	3.35

terrigenous mineral in aqueous flow. Chlorite ranges from 3.91 to 8.90% in the samples. Chlorite is formed probably as a ferrous iron magnesium aluminosilicate.

3.10. Geochemical data

The values of major, trace and rare earth elements contents of the ironstones obtained from the present investigation are presented in Tables 2–4. The ironstones consist of SiO_2, Fe_2O_3 and Al_2O_3 which are the most enriched oxides and make up to 70% of the oxides in all the samples. This appears to be a reflection of the predominance of siderite, hematite, clay minerals and quartz in the ironstone samples. Range of values of major elements obtained from the samples are; Fe_2O_3 (41.50–54.60%), SiO_2 (6.10–23.30%), Al_2O_3 (3.64–7.00%), CaO (1.40–13.60%), MgO (0.30–1.20%) and P_2O_5 (0.10–8.80%). It is important to note that many of the samples analyzed show relatively high concentration of MgO, CaO and P_2O_5. An interesting spike in the concentration of Pb, Zn, Ni and Co is also observed in some of the intervals (Samples JAH1JA and JAH1JB) at the lower part of the section at Ahoko quarry. The same intervals show distinctly high concentration of MgO, P_2O_5 and CaO also (Tables 2 and 3). The reverse is the case in the other lithofacies of the ironstones, particularly up section. At Idu, the concretional ironstone facies is characterized by exceptionally low CaO, MgO and P_2O_5 (less than 0.01) and enrichment in SiO_2. A comparison of the trace element composition of the ironstones with the host shales (Table 5) shows close similarity.

The rare earth elements data obtained from the investigated ironstones are presented in Table 4. The total REEs contents of the samples range from 32.2 ppm to 259.53 ppm. The total REEs contents are moderate (generally more than 80 ppm) with the exception of only sample JID1A with less than 32.2 ppm. They are enriched in light rare earth elements (LREE) contents (30.00–217.52 ppm) but depleted in the heavy rare earth elements (HREE) contents (2.93–41.77 ppm). Plot of concentrations of the rare earth elements and yttrium (REE + Y) normalized to North American Shale Composite (NASC; Gromet et al. (1984) is shown in Fig. 8 and it shows a flat pattern. Positive Ce anomaly (1.00–1.38) was obtained for all the studied samples. Positive Eu anomaly was recorded for most samples but negative values were also recorded for few samples (Table 4). The investigated ironstones show enrichment in Nd concentrations (10–100 ppm) with an exception of sample JID1A (6.66 ppm).

4. Discussion

4.1. Diagenesis

The field, mineralogical and geochemical data obtained from the present investigation of ferruginous samples provided evidences that they are sideritic and diagenetic. The rhythmitic bedding of the host shale-clay facies, occurrence of the ironstone in form of traceable and laterally persistent bands, concretions and lenses within the argillaceous beds suggest that they were formed at the bedding planes between the argillaceous beds (Figs. 3 and 4). This position is supported by the strong similarity in depositional features of the ironstone with the host shales. They are interpreted to have been formed as a replacement and of precipitation of hematite and siderite as early diagenetic products from iron rich water migrating through the bedding planes and fractures under reducing condition (Browne and Kingston, 1993; Afify et al., 2018).

The similarity in the chemical composition of the host shales and the ironstones (Table 5) attest to the role of the host shale as precursor in the formation of the ironstones through diagenetic process shortly after deposition (Akinlotan, 2017; Afify et al., 2018). Evidence of the influence of migrating pore water and precipitation of sideritic minerals under anoxic condition is exhibited by the formation of the secondary iron minerals in vertical fractures in form of clastic dykes in the shales (Fig. 4D). The structural disposition of the vertical fractures in which they cut through the shale beds but terminate at the base of the ironstone is part of the evidences that the ironstones are post depositional and diagenetic. The vertical fractures preceded the ironstone and also serve as conduits for the iron rich migrating fluids, from which most of the iron minerals precipitated.

The diagenetic process probably began very shortly after the sediments were deposited (Fig. 9) and presumably the bedding planes which appear more porous and permeable allowed the iron rich fluid migration during early stage of burial and subsequent compaction. The water between the sediment intergranular spaces were probably enriched with Ca and Mg dissolved from gastropods and bivalves preserved in the host shales (Fig. 6A and D) and also partly sourced from normal sea water (Akinlotan, 2019). The high amount of MgO and CaO in the ironstones is an evidence that they were sourced originally in the sediments from sea water. Previous work on the adjacent Agbaja ironstone indicated that they were so depleted in the oxides indicating that they are different in term of origin (Ladipo et al., 1994; Mücke 2006).

Plants and other materials within the sediment got decomposed and the initial pore water becomes more acidic. Acidic water then dissolved the calcite which is the main constituent of bioclasts, therefore releasing calcium and carbonate ions into the water between the sand and silt grains (Mücke 2006; Loope et al., 2012). This was succeeded by decomposition of organic matter which is believed to have led to reduction in the dissolved oxygen in the water trapped between the sediment grains. The iron also became more soluble and was leached out of the minerals. The dissolved mineral matter (mainly calcium, iron, and carbonate) were trapped in sites within the sediment where they are less soluble and precipitated out either as siderites between the intergranular pore and fractures in the original shale or as replacement in the clayey sediments which are essentially kaolinite (Figs. 6 and 9).

4.2. Genesis, depositional environments and paleogeography

Available data in this study suggest possibility that most of the argillaceous sediments were deposited primarily out of suspension in a quiet freshwater to open marine environment and the sediments were probably sourced from the adjacent Lower-Proterozoic to Precambrian basement complex. Intense weathering would have lead to the release of the free iron which migrates with the pore water through the more permeable discontinuities (bedding planes and fractures) upon burial

Table 3
Trace Elements (ppm) composition of the investigated ironstone.

Sample	Sc	V	Ba	Sr	Zr	Cr	Co	Ni	Cu	Zn	As	Pb
JAH1B	4.40	33.00	90.50	60.10	5.40	16.40	6.20	5.20	5.02	25.00	1.10	8.49
JAH1N	6.10	25.00	100.10	45.20	12.10	18.20	17.50	11.90	6.07	70.60	1.40	9.78
JAH1R	5.90	25.00	93.00	45.40	10.60	17.20	14.30	10.00	5.58	54.30	1.50	12.75
JAH1T	12.80	60.00	165.60	119.40	7.50	16.60	13.60	9.40	4.45	61.10	1.10	12.80
JAH1JA	32.70	93.00	323.30	469.80	2.60	26.60	50.50	23.90	6.55	178.50	2.20	18.56
JAH1JB	38.90	62.00	483.10	1065.80	3.60	20.80	22.90	11.30	4.45	128.90	1.60	26.86
BGH1C	6.60	25.00	225.10	179.10	7.60	12.70	12.20	6.90	4.11	45.70	1.10	16.22
BGH1E	4.30	21.00	103.40	65.30	8.90	15.70	16.00	9.00	4.78	65.20	1.00	12.37
JID1A	1.10	42.00	15.70	6.00	6.10	25.60	0.80	2.80	14.22	31.00	<0.1	27.78

Table 4
Rare Earth Elements (ppm) composition of the investigated ironstone.

Sample	JAH1B	JAH1N	JAH1R	JAH1T	JAH1JA	JAH1JB	BGH1C	BGH1E	JID1A
La	14.30	21.10	18.50	26.10	48.40	51.70	15.70	16.10	5.10
Ce	46.90	51.00	44.30	62.30	104.70	91.00	36.70	38.50	15.10
Pr	4.01	5.62	4.74	6.74	11.25	9.25	3.91	4.36	1.74
Nd	16.33	22.34	18.93	29.17	44.16	34.33	15.09	18.14	6.66
Sm	3.34	4.59	4.20	6.50	9.01	6.57	3.22	4.50	1.40
Eu	0.70	1.29	0.94	1.52	2.15	1.74	0.76	1.02	0.27
Gd	2.56	5.82	4.41	7.68	10.42	8.70	2.66	5.13	0.94
Tb	0.40	0.91	0.77	1.21	1.70	1.53	0.51	0.82	0.19
Dy	2.30	5.26	4.78	6.98	9.85	10.06	2.92	3.87	0.80
Ho	0.40	1.11	0.96	1.51	2.40	2.49	0.69	0.99	0.11
Er	0.88	2.74	2.59	3.98	7.05	8.24	1.82	2.38	0.47
Tm	0.18	0.39	0.34	0.55	1.00	1.31	0.20	0.34	0.05
Yb	1.05	2.29	2.07	3.83	6.45	8.10	1.58	1.99	0.32
Lu	0.14	0.30	0.28	0.48	0.99	1.34	0.27	0.27	0.05
ΣREE	93.49	124.76	107.81	158.55	259.53	236.36	86.03	98.41	33.20
ΣLREE	84.88	104.65	90.67	130.81	217.52	192.85	74.62	81.60	30.00
ΣHREE	7.91	18.82	16.20	26.22	39.86	41.77	10.65	15.79	2.93
ΣLREE /ΣHREE	10.73	5.56	5.60	4.99	5.46	4.62	7.01	5.17	10.24
Eu/Eu*	1.38	1.06	1.09	0.84	0.73	0.84	1.43	1.01	2.20
Ce/Ce*	1.38	1.05	1.06	1.02	1.00	0.89	1.06	1.02	1.23

Table 5
Comparison of Trace elements (ppm) values the ironstone and shale of the Patti Formation.

Trace elements	Ironstone (Current study)	Shale (Okunlola and Idowu, 2012)	Shale (Ojo et al., 2016)
Ba	177.76	394.23	371.25
Sr	228.46	59.39	150.18
Ni	10.04	19.37	11.00
Co	17.11	33.42	14.49
Cu	6.14	14.45	11.79
Zn	73.37	116.39	84.06
V	42.89	108.77	101.81
Y	45.15	70.69	60.59
Zr	7.16	1156.54	659.11
Mo	0.41	0.72	0.41
Nb	1.89	52.46	35.44
Pb	27.78	22.28	19.99
Rb	2.48	46.19	35.13
Th	6.57	29.22	17.58
U	2.67	13.07	10.14
Cu/Zn	0.08	0.12	0.14
(Cu + Mo)/ Zn	0.09	0.13	0.15
Ni/Co	0.59	0.58	0.76
Rb/K_2O	8.00	32.23	43.37
U/Th	0.41	0.45	0.58

and compaction (Rodrigues et al., 2015).

The siderites and iron oxide minerals were subsequently precipitated mainly from diagenetic modifications (Fig. 9). Our field, chemical, and mineralogical evidences pointed to a suite of diagenetic modifications (compaction, dewatering, dissolution, organic matter decomposition, replacement and mineral precipitation) involved in the formation of the sideritic ironstones under reducing condition (Fig. 9) (Akinlotan, 2019). According to (Mücke, 2006) fine grained sediments containing organic matter are decomposed resulting in highly reducing anoxic environment in which abundant siderite are formed. Oxidation of the organic materials creates a conducive condition for iron reduction and in the process ferrous iron and carbon dioxide are generated. Several authors (Pye et al., 1990; Isaack et al., 2017; Akinlotan, 2019) have advanced positions that occurrence of siderite is an indication of reducing condition and it is favoured where sulfate reducing bacteria are present and active and it forms when Fe reduction is higher than sulfate reduction.

Mineralogical and geochemical evidences show that the investigated ironstones which are essentially sideritic fall in the carbonate zone (Fig. 10) with little contribution of silicate from the oxide zone. Mücke et al. (1999) identified siderite as index mineral that indicates sediments which are diagenetically form in anoxic environment. Very low Eh-pH condition is another conditions required for the formation of siderite e.g. $FeCO_3$ precipitates from Fe^{2+} bearing solution under low Eh (v) from 0 to −0.6 and pH from 6.5 to 9 (Brooklins, 1988). The presence of chlorite presumably indicates that we have Calcite series with end members like calcite, siderite and magnetite and the chlorite series, though our XRD did not pick up chamosite (Mücke, 2006).

The low concentration of Cu, Pb and Zn in the analyzed samples coupled with observed insignificant correlation of Fe with As, Cu, and Zn do not favour hydrothermal precipitation as a mechanism of formation (Lottermoser and Ashley, 1996; Ashley et al., 1998; Gloaguen et al., 2007). The plot of Si versus Al after Crerar et al. (1979) is in support of diagenetic origin for the ironstones (Fig. 11). The origin of the investigated ironstones was further constrained using REEs data. The REE contents in the samples ranges from 93.49 ppm to 259.53 ppm except sample JID 1A from Idu section. These values fall within the range of the ferromanganese deposits of diagenetic origin (110–489 ppm) and it is closely compared to the Upper Cretaceous ironstones in the Bahariya depression of Egypt with total REE content ranging from 70 to 348 ppm (Afify et al., 2018). The total REE contents of the studied ironstones (32.26–348.87 ppm) fall within the range of the ferromanganese deposits of diagenetic origin (110–489 ppm). Usui et al. (1997), Bau et al. (2014) and Garnit and Bouhlel (2017) suggested that low total REEs (<100 ppm) characteristics of ironstone from hydrothermal origin and therefore the Patti ironstones do not fit into hydrothermal origin model. The similarity with the Upper Cretaceous ironstones in the Bahariya depression of Egypt is demonstrated by relatively high Nd concentrations which range from 10 to 100 ppm and flat REE + Y pattern which imply diagenetic origin (Afify et al., 2018). Eu and Ce anomalies recorded from the Patti ironstones are however slightly positive and this may indicate some level of influence of hydrogenetic origin.

The observed spikes in the concentration of the MgO, CaO and the relics of marine gastropod and bivalve shells preserved at the lower part of the investigated sections show that the precursor shales at the intervals probably represent the maximum flooding surface in the basin. Geochemical proxies like the binary plot of Na against Mg shows most of the Patti samples plotted in the shallow marine field except sample JID1A from Idu (Fig. 12). The chemical data shows that the ironstones with composition largely reflecting the primary host rocks are of two types; the marine sideritic and fresh water sideritic ironstones (Akinlotan, 2019). Full marine sideritic ironstone is most likely to have been

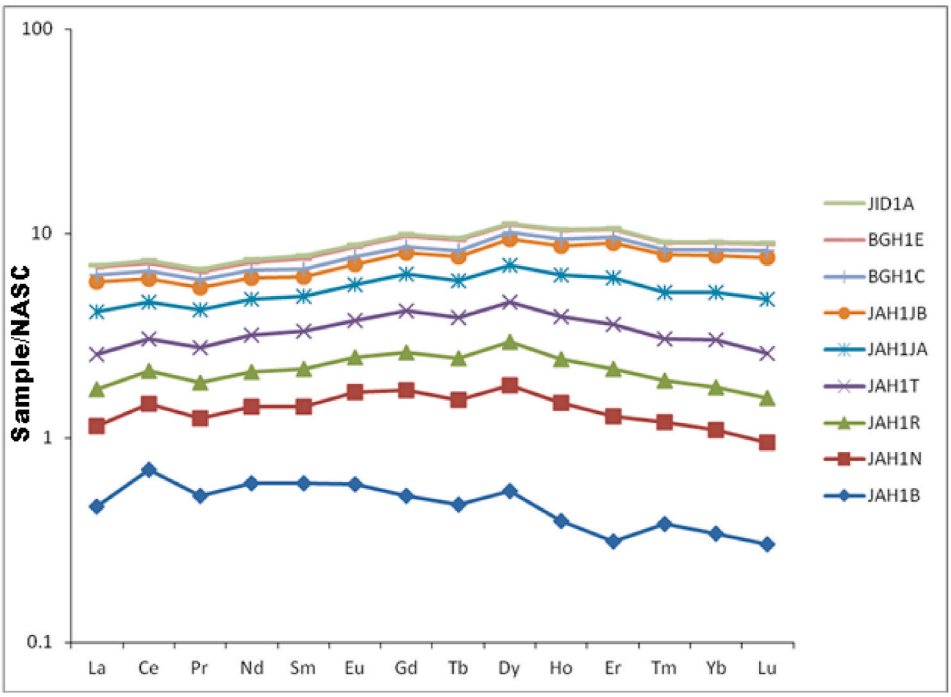


Fig. 8. NASC-normalized (Gromet et al., 1984) REE distribution patterns for the Patti Formation Ironstone.

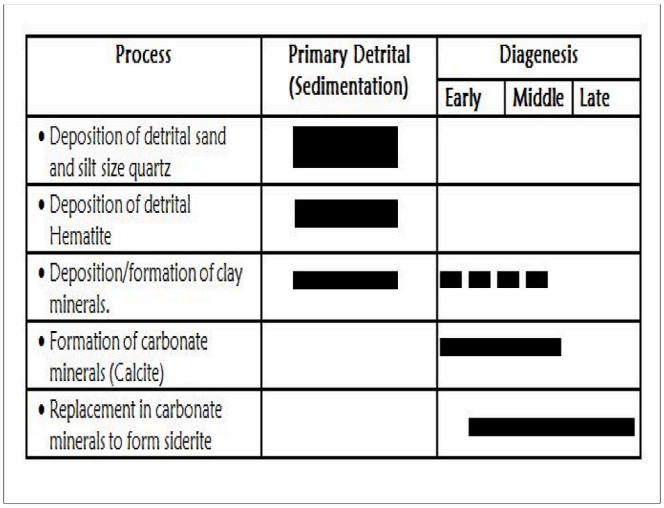


Fig. 9. Paragenetic sequence of the investigated ironstones.

established at the lower part of the investigated section where the laminated facies is relatively high in MgO, P_2O_5 and CaO at Ahoko and Geheku.

To further assess the paleoenvironmental condition a plot of V versus Ni was made (Fig. 13) and it shows the studied samples fall within marine anoxic and marine-terrestrial fields (Akinlua et al., 2016). Up section, there was fluctuation and shallowing of water salinity which is reflected in the drop in the amount of CaO and MgO of the ironstones. The evidence of non marine or fresh water condition is indicated by a sharp drop in the in the concentration of MgO, CaO and trace elements like V, Zn and Ni in the samples up section. The presence of fresh water siderite is also an evidence. At Idu section, the very low amount of Mg and Ca but high Si in the ironstone is indicative of freshwater influence. Field evidence like preserved gastropod and pelecypod shells which are essentially marine faunal is a pointer to deposition of the ironstones of Patti Formation in shallow marine environment with prevailing reducing condition. It is important to mention here that the above scenario lends credence to the previous assertion that sideritic ironstones are useful as paleoenvironmental indicator (Choi et al., 2003; Lim et al., 2004; Akinlotan, 2019). This study is supportive of the suggestions of an earlier work that interpreted the lithofacies assemblage (shale, claystone and the ironstone) of the Patti Formation in the present study area as fresh water to nearshore marine deposits. Ojo and Akande (2006, 2009) reported that the fossiliferous shales and the ferruginous facies which contain marine mollusk shells and ophiomorpha burrows in the present study area as marine flooding surface whereas the overlying coaly shale, lignitic beds and kaolinitic clays as freshwater proximal deltaic plain and floodplains.

On a regional paleogeograhic context, the implication therefore from the aforementioned evidences is that there was marine incursion into this part of the Bida Basin in the Maastrichtian times. It was short-lived and reached its peak and followed by intermittent river run offs which developed non marine swamps. The palynological analysis of shales associated with the marine sideritic ironstone shows presence of marine dinocysts like Dinogymnium, Spiniferites and Senegalinium (Ojo and Akande, 2006, 2008). We therefore suggest that study area is very important with respect to paleogeographic history of the Bida Basin as evidences of sea incursion; maximum flooding surface and regression are preserved in the studied sections. The indication of anoxic condition also revealed by the sideritic ironstone is of exploration strategy in terms of hydrocarbon source rocks potential in a relatively untested basin like Bida Basin. Anoxic conditions are favourable for preservation of organic matter and excellent source rock formation. Ojo et al. (2018) reported excellent source rocks from these intervals and there may be prospects of very organic rich intervals associated with the anoxic event in the deeper subsurface levels.

4.3. Comparison with other ironstones

To further illustrate and examine the significance of the present study locally and regionally, we attempt a comparison of the investigated ironstone of the Patti Formation (present study) with Agbaja and Batati ironstones (Bida Basin, Nigeria), Leru ironstone (Anambra Basin, Nigeria), Weald Basin ironstone (England) and Bahariya ironstone

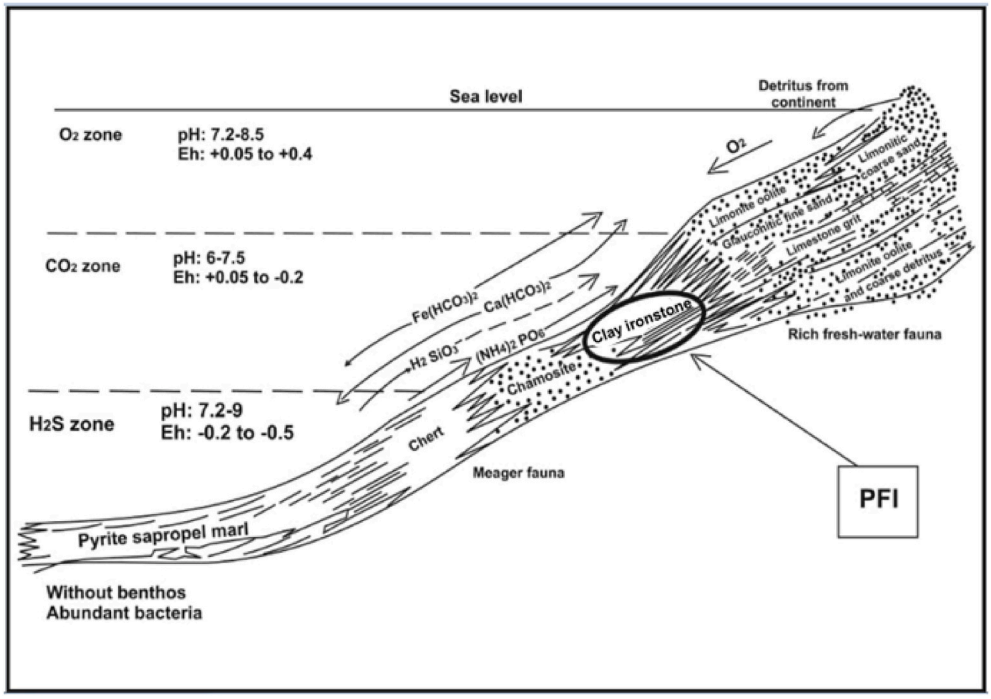


Fig. 10. Schematic section illustrating the physicochemical conditions that favoured the formation of the investigated ironstones after Borchert (1960) and Pettijohn (1975).

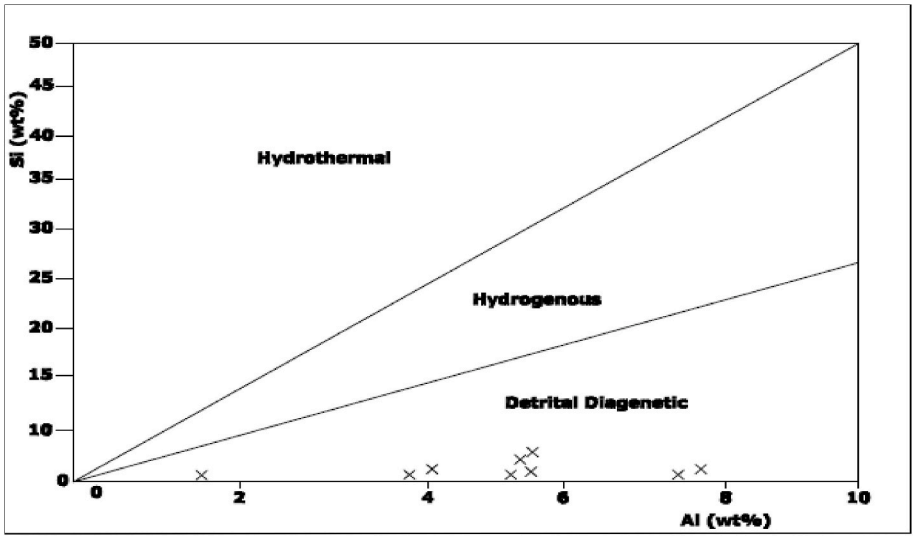


Fig. 11. Discriminative bivariate plot of Si versus Al revealing diagenetic origin for the investigated ironstones (Crerar et al., 1979; Crerar et al., 1982).

(Egypt) in respect of age, mode of occurrence, mineralogy, elemental composition and origin (Table 6). The results show that the Agbaja and Batati ironstones are different from the ironstones of the Patti Formation at Ahoko and Geheku. First observation is that the Patti ironstones at Ahoko and Geheku are not oolitic like Agbaja and Batati but rather occur as parallel laminated, fossiliferous, concretional and massive bands within the host shales and show good similarity with the shale interbeds. Basically Agbaja ironstone is younger than ironstone of the Patti Formation and the mode of origin is different. However, these features exhibited by the Patti Ironstones are also rather shared with the Maastrichtian Leru ironstone, Lower Cretaceous Weald basin ironstone and that of Cenomanian ironstone of Bahariya Egypt. Mücke (2000) explained that the ooidal structures of the Agbaja Ironstone were mechanically formed through reworking processes caused by high energy tidal waves in a marginal environment. It should be noted that the ironstones under study were deposited under more quiet condition.

Compositionally, the Patti ironstones at Ahoko are relatively enriched with MgO and Cao like the Leru ironstones (≤8.50% and 13.97% respectively), whereas Weald Basin ironstones show absence of Mgo and CaO up to 2.30% and the Agbaja Ironstone is exceptionally low in MgO and CaO or even absent (Akande and Mücke 1993; Mücke, 2000: Akinlotan, 2019). Siderite constitutes the major component of the Patti ironstone and Weald Basin. They are therefore sideritic ironstones but Agbaja ironstones have very low amount of siderite and more of kaolinite and goethite (Mücke, 2000). In Bahariya ironstones, siderite occurs as a subordinate amount, whereas Fe-dolomite, ankerite, goethite and hematite are the main iron-bearing minerals (Afify et al., 2015). Leru ironstone is both sideritic and chamositic.

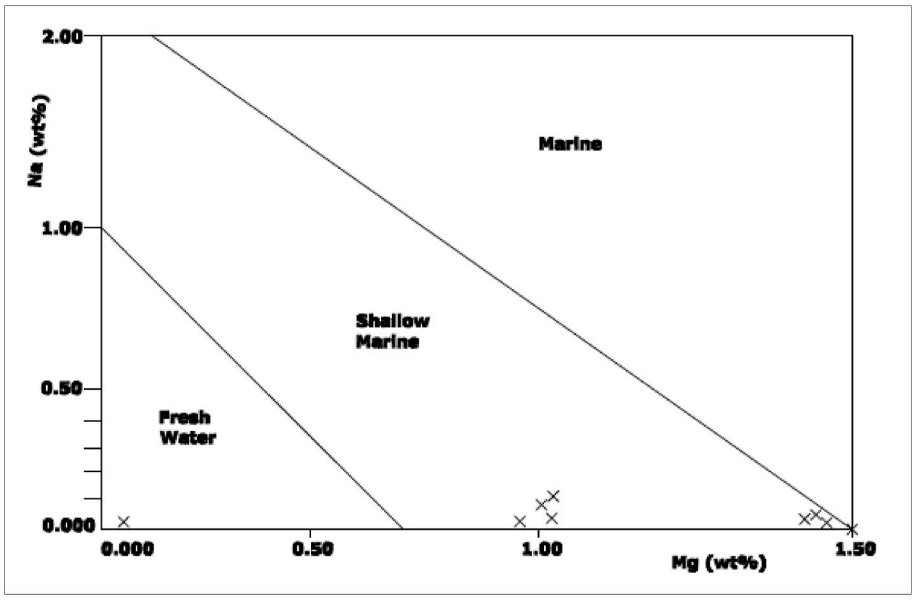


Fig. 12. Discriminative binary plot of Na against Mg after Nicholson (1992). Note most of the investigated ironstone samples fall within the shallow marine field.

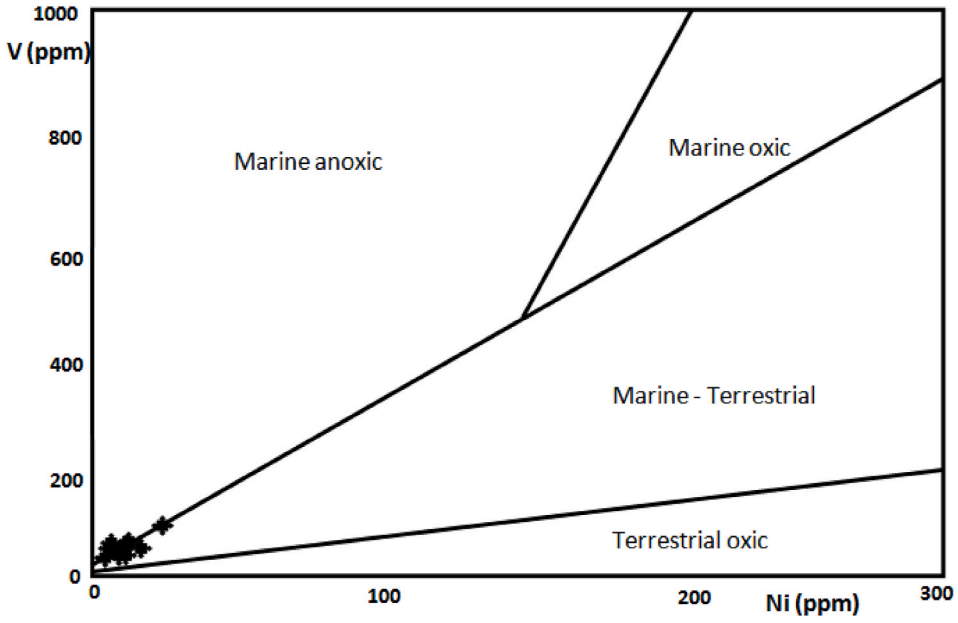


Fig. 13. Discriminative binary plot of Ni vs. V. Note that the investigated ironstone samples fall within marine environments (after Akinlua et al., 2016).

The paleogragraphic implication is that all the ironstones reviewed are diagenetic in origin and formed under various level of reducing conditions. While the elemental composition of the Agbaja and Weald basin ironstones indicate that they were formed in a very low salinity to fresh water condition, the Patti ironstones at Ahoko (Bida Basin) and Leru (Anambra basin) indicate more full saline water (Mücke 2000; Akinlotan, 2019). It is important to note that the two are fossiliferous containing marine bioclasts of bivalves and gastropods. Even though chamositic clay was not picked up by the XRD peaks of the Patti ironstones like the Leru but high MgO and magnesian siderite were recorded. There is possibility therefore, that Mg and Ca would have been impacted on the primary shale materials by sea water and those dissolved from the calcareous bioclasts.

The Patti ironstones under investigation in this study fit more into the Chamosite type ironstone deposit like that of the Leru and Aswan of Egypt (Mücke, 2006) rather than the kaolinite type which the adjacent Agbaja ironstone belonged. Previous biostratigraphic studies of the host shale by Ojo and Akande (2006) showed the occurrence of marine dinocysts assemblage and microforaminiferal lining at the lower part of Ahoko section indicating peak of marine flooding of the Bida Basin at this interval. The present study further provides evidence of influence of marine water in the deposition of the Patti shales as against the earlier interpretation of Braide (1992) which ascribed the shales as deposits of fluvial origin. As pointed out by Akinlotan (2019), the sideritic ironstone could be an additional tool to constrain the paleogeographic settings of depositional basins. In deed the findings in this study show the assertion is valid and applicable in our study area. Further paleogragraphic implication of this study is that the similarity in the composition of the Patti ironstone with that of the Leru in Anambra Basin is an indication of possible connection between the Gulf of Guinea sea in the south with the Tethys sea through the Bida Basin in the Maastrichtian (Ojo and Akande, 2006).

Table 6
Comparison of the studied ironstone with other ironstones from some selected locations.

Features		Locations					
		Patti Ironstone, Bida Basin (Present Study)	Agbaja, Bida Basin Nigeria (Mücke, 2000)	Batati, Bida Basin, Nigeria (Mücke, 2000)	Leru, Anambra Basin, Nigeria (Mücke, 2000)	Bahariya, Egypt (Afify et al., 2018)	Weald basin, England (Akinlotan, 2019)
Age		Maastrichtian	Maastrichtian to Paleocene?	Maastrichtian	Maastrichtian	Cenomanian (Host rock) and Coniacian to Turonian (ironstone)	Lower Cretaceous
Field Characteristics; Texture/structure		Spheroidal concretional; massive bioturbated; and laminated and fossiliferous; and occur within shales	Thick oolitic to pisolitic	Oolitic/Pisolitic	Bioturbated and fossiliferous; oolitic, bands within shales	Thin massive bands; concretions within siliciclastic rocks	Nodular, tabular and spherulitic; interbedded with mudstones and sandstones
Mineral Composition		Siderite, magnesian siderite, kaolinite and hematite	Kaolinite type, goethite and apatite	Kaolinite, goethite, hematite and minor siderite	Siderite, Chamosite type	Goethite, hematite, dolomite, ankerite and minor siderite	Siderite, illite and kaolinite
Geochemistry Major Elements (wt.%)	**CaO**	1.41–13.97	Absent to low	0.00–0.22		≤12	0.30–2.30
	MgO	1.82	0.00–0.40		0.50–6.75	≤8.50	0
	Fe_2O_3	36.46–47.48	36–74			Up to 73	64–73
Fluid Migration		Active roles of meteoric water and sea water. Fractures and bedding planes as migration pathways	Ferruginization through meteoric water	Ferruginization through meteoric water	Influence of seawater	Influence of meteoric water enhanced by organic matter decomposition and HC migration. Fractures and permeable rocks as conduits	Active roles of meteoric water and bacterial activities. Discontinuities as migration pathways for fluids
Origin		Post depositional diagenetic modification under anoxic freshwater-full marine condition	Replacement of kaolinite by goethite in low salinity water	Replacement of kaolinite by goethite in low salinity water	Full marine condition	Diagenetic origin. Replacement of host by iron bearing minerals	Post depositional diagenetic modification. freshwater anoxic conditions

Generally, in our study area, field evidences such as closely spaced vertical fractures cutting through the shales, occurrence of the ironstones at the bedding planes of the host beds and similarity of the composition and sedimentary features of the primary shale with the investigated ironstones is consistent with the mechanism of replacement or ferruginization related to the migration of iron rich fluids through pathways provided by permeable bedding planes and vertical fractures and consequent precipitation under the influence of anoxic condition (Afify et al., 2018). This mechanism correlates positively with the Weald Basin and Cenomanian Bahariya ironstones of Egypt.

5. Conclusions

The geologic field investigation reveals that the ironstones of the Maastrichtian Patti Formation consist of laminated fossiliferous ironstone, spheroidal and concretionary ironstone facies, and massive, bioturbated ironstone facies and they were formed at the bedding planes of the shale and the clay beds. The host shales are cut by vertical fractures which served as conduits for the migrating iron rich porewater.

Petrography and XRD results show the dominance of siderite, quartz, kaolinite, chlorite and hematite in the analyzed ironstones. The data suggest that kaolinites were replaced by siderite in an environment depleted of oxygen at shallow burial and early stage of diagenesis.

Geochemical proxies suggest the precursors are deposited in normal seas but with occasional influence of fresh water in an anoxic setting. Intervals with the relatively high concentration of Cao, MgO, V, Zn and Pb at the lower part of the section may represent maximum flooding surface.

Generally the study suggests that the ironstones are sideritic and diagenetic. Majority of the ironstone contain marine siderites whereas few intervals are of freshwater siderite. The Maastrichtian sea in the basin was shallow, short-lived and truncated by intermittent river run offs. The study further provides indication of connection between the Anambra and Bida Basins and presumably a link between the Tethys and the Gulf of Guinea seas in the Maastrichtian.

Declaration of competing interest

The authors declare that they have no known competing financial interests or personal relationships that could have appeared to influence the work reported in this paper.

Acknowledgements

We acknowledge the Federal University Oye-Ekiti, Nigeria for the financial support for the fieldwork courses of the Department of Geology during which the field aspect of this study was carried out. This paper was written during the sabbatical tenure of the first author with the Department of Geology and Mineral Sciences, Kwara State University, Malete, Nigeria. Our appreciation goes to the authority of the two institutions. We like to thank the anonymous reviewers for their invaluable suggestions which have unarguably impacted the quality of this article.

Appendix A. Supplementary data

Supplementary data related to this article can be found at https://doi.org/10.1016/j.jafrearsci.2020.104058.

References

Abimbola, A.F., Badejoko, T.A., Elueze, A.A., Akande, S.O., 1999. The Agbaja ironstone formation, nupe basin, Nigeria – a product of replacement of a kaolinite precursor. Global J. Pure Appl. Sci. 5, 375–384.

Adeleye, D.R., 1973. Origin of ironstones, an example from the Middle Niger basin, Nigeria. J. Sediment. Petrol. 43 (3), 709–727.

Afify, A.M., Sanz-Monteroa, M.E., Calvo, J.P., 2018. Differentiation of ironstone types by using rare earth elements and yttrium geochemistry – a case study from the Bahariya region, Egypt. Ore Geol. Rev. 96, 247–261.

Afify, A.M., Sanz-Montero, M.E., Calvo, J.P., Wanas, H.A., 2015. Diagenetic origin of ironstone crusts in the lower cenomanian Bahariya formation, Bahariya depression, western desert Egypt. J. Afr. Earth Sci. 101, 333–349.

Akande, S.O., Mücke, A., 1993. Depositional environments and diagenesis of carbonates of the mamu/nkporo formation transition, Anambra basin, southern Nigeria. J. Afr. Earth Sci. 17 (4), 445–456.

Akinlotan, O., 2017. Multiproxy approach to paleoenvironmental modelling: the English lower cretaceous Weald basin. Geol. J. https://doi.org/10.1002/gj.2893.

Akinlotan, O., 2019. Sideritic ironstones as indicators of depositional environments in the Weald basin (early cretaceous) SE england. Geol. Mag. 156 (3), 533–546.

Akinlua, A., Olise, F.S., Akomolafe, A.O., McCrindle, R.I., 2016. Rare earth element geochemistry of petroleum source rocks from north-western Niger Delta. Mar. Petrol. Geol. 77, 409–417.

Ashley, M.P., Lootermosser, B.G., Westaway, J.M., 1998. Iron formations and epigenetic ironstones in the paleoproterozoic Willyama supergroup, Olary domain, South Australia. Min. Pet. 64, 187–218.

Bau, M., Schmidt, K., Koschinsky, A., Hein, J., Kuhn, T., Usui, A., 2014. Discriminating between different genetic types of marine ferro-manganese crusts and nodules based on rare earth elements and yttrium. Chem. Geol. 381, 1–9.

Borchert, H, 1960. Genesis of marine sedimentary iron ore. Inst. Min Metall. Bull. 69, 261–279.

Braide, S.P., 1992. Syntectonic fluvial sedimentation in the central Bida Basin. J. Min. Geol. 28, 55–64.

Brooklins, D.G., 1988. Eh-PH Digrams for Geochemistry. Springer Verlag, Berlin, p. 176.

Browne, G.H., Kingston, D.M., 1993. Early diagenetic spherulitic siderites from pennyslavania palaesols in the boss point formation, maritime Canada. Sedimentology 40, 467–477.

Choi, K.S., Khim, B.K., Woo, K.S., 2003. Spherulitic siderites in the Holocene coastal deposits of Korea (eastern Yellow sea): elemental and isotopic composition and depositional environment. Mar. Geol. 202, 17–31.

Crerar, D.A., Knox, G.W., Means, J.L., 1979. Biogeochemistry of bog iron in the New Jersey pine barrens. Chem. Geol. 24, 111–136.

Crerar, H.D., Namson, M.S., Chyi, L., Feigensen, M.D., 1982. Manganiferous cherts of the Franciscan assemblage: I general geology, ancient and modern analogues and implications for hydrothermal convection at oceanic spreading centers. Econ. Geol. 77, 519–540.

Curtis, C., Pearson, M., Somogyi, V., 1975. Mineralogy, chemistry and origin of a concretionary siderite sheet (clay-ironstone band) in the Westphalian of Yorkshire. Mineral. Mag. 40, 385–393.

Garnit, H., Bouhlel, S., 2017. Petrography, mineralogy and geochemistry of the late eocene oolitic ironstones of the jebel ank, southern Tunisian atlas. Ore Geol. Rev. 84, 134–153.

Gloaguen, E., Branquet, Y., Boulvais, P., Moelo, Y., Chauvel, J.J., Chiappero, P.J., 2007. Palaeozoic oolitic ironstone of the French Armorican Massif: a chemical and structural trap for orogenic base metal–As–Sb–Au mineralization during Hercynian strike-slip deformation. Miner. Deposita 42, 399–422.

Gromet, L.P., Dymek, R.F., Haskin, L.A., Korotev, R.L., 1984. The North American shale composite. Its compilation, major and trace element characteristics. Geochem. Cosmochim. Acta 48, 2469–2482.

Isaack, A., Gischler, E., Hudson, J.H., Anselmetti, F.S., Buhre, S., Camoin, G.F., 2017. Facies variations in response to Holocene sea level and climate change on Bora Bora, French Polynesia: unraveling the role of synsedimentary siderite in a tropical marine, mixed carbonate-siliciclastic lagoon. Mar. Geol. 390, 1–22.

Jones, H.A., 1958. The oolitic ironstones of Agbaja plateau, kabba province. Record of the Geological Survey of Nigeria, pp. 20–43.

Kogbe, C.A., 1976. Paleographic history of Nigeria from Albian times. In: Kogbe (Ed.), Geology of Nigeria-Elizabeth Publish Co, pp. 237–252.

Ladipo, K.O., Akande, S.O., Mücke, A., 1994. Genesis of ironstones from the Middle Niger sedimentary basin, evidence from ore microscopic and geochemical studies. J. Min. Geol. 30, 161–168.

Lim, D.I., Jung, H.S., Yang, S.Y., Yoo, H.S., 2004. Sequential growth of early diagenetic freshwater siderites in the Holocene coastal deposits, Korea. Sediment. Geol. 169, 107–120.

Loope, D.B., Kettler, R.M., Webber, K.A., 2012. Morphologic clues to the origins of iron oxide–cemented spheroids, boxworks, and pipelike concretions, Navajo Sandstone of South-Central Utah. U.S.A. Journal of Geology 119, 505–520.

Lottermoser, B.G., Ashley, P.M., 1996. Geochemistry and exploration significance of ironstones and barite-rich rocks in the proterozoic willyama supergroup, olary block, south Australia. Journal of Geochemistry Explorer 57, 57–73.

Mücke, A., 2000. Environmental conditions in the late Cretaceous African Tethys: conclusions from a microscopic-michrochemical study of ooidal ironstones from Egypt, Sudan and Nigeria. J. Afr. Earth Sci. 30, 25–46.

Mücke, A., 2006. Chamosite, siderite and the environmental conditions of their formation in Chamosite-Type Phanerozoic ooidal ironstones. Ore Geol. Rev. 28, 235–249.

Mücke, A., Badejoko, T.A., Akande, S.O., 1999. Petrographic, mechanical studies and origin of Agbaja Phanerozoic ironstone formation, Nupe Basin, Nigeria: a product of ferruginised ooidal kaolin precursor not identical to the Minette type. Miner. Deposita 34, 284–296.

Nicholson, K., 1992. Genetic types of manganese oxide-deposits in Scotland: indicators of Paleo-ocean spreading rate and a Devonian Geothermal mobility boundary. Econ. Geol. 87, 1301–1309.

Ojo, O.J., Akande, S.O., 2006. Sedimentological and palynological studies of the Patti formation, southeastern Bida basin, Nigeria: implications for paleoenvironments and paleogeography. Nigerian Association of Petroleum Explorationists Bulletin 19, 61–77.

Ojo, O.J., Akande, S.O., 2008. Microfloral assemblage, age and palaeoenvironment of the upper cretaceous Patti Formation, south-eastern Bida Basin, Nigeria. J. Min. Geol. 44 (1), 71–78.

Ojo, O.J., Akande, S.O., 2009. Sedimentology and depositional environments of the maastrichtian Patti Formation, south-eastern Bida Basin, Nigeria. Cretac. Res. 30, 1415–1425.

Ojo, O.J., Babatunde, F.R., Adepoju, S.A., Akande, S.O., Momoh, A., 2016. Provenance and weathering history of the maastrichtian shale member of the Patti Formation, southern Bida Basin, Nigeria. J. Geol. Soc. India 88, 471–480.

Ojo, O.J., Jimoh, A.Y., Umelo, J.C., 2018. Geochemical and palynological studies of some maastrichtian source rock intervals (Patti and gombe formations) in Nigeria: implications for hydrocarbon prospectivity. AAPG Search and Discovery (2019). Article #11185.

Ojo, S.B., Ajakaiye, D.E., 1989. Preliminary interpretation of gravity measurements in the middle Niger Basin area, Nigeria. In: Kogbe, C.A. (Ed.), Geology of Nigeria, second ed. Elizabethan Publishing Company, Lagos, pp. 347–358.

Okunlola, O.A., Idowu, O., 2012. The geochemistry of claystone-shale deposits from the maastritchian Patti Formation, southern Bida Basin, Nigeria. Earth Sci. Res. J. 16 (2), 57–67.

Pettijohn, F.J., 1975. Sedimentary Rocks, second ed. Harper Bros, New York, N.Y., p. 718

Pye, K., Dickson, J.A.D., Schiavon, N., Coleman, M.L., Cox, M., 1990. Formation of sideritic-Mg-calcite-iron sulphide concretions in intertidal marsh and sandflat sediments, Northfolk, England. Sedimentology 37, 325–343.

Rodrigues, A.G., De Ros, L.F., Neumann, R., Borghi, L., 2015. Paleoenvironmental implications of early diagenetic siderites of the Paraiba do Sul Deltaic complex, eastern Brazil. Sediment. Geol. 323, 15–30.

Udensi, E.E., Osazuwa, I.B., 2004. Spectra determination of depths to magnetic rocks under the nupe basin, Nigeria. Nigerian Association Petroleum Explorationists Bulletin 17, 22–37.

Usui, A., Bau, M., Yamazaki, T., 1997. Manganese microchimneys buried in the Central Pacific pelagic sediments: evidence of intraplate water circulation? Mar. Geol. 141, 269–285.

Yasin, A.T., 2009. Mineralogy Petrography and Geochemistry of Iron Rich Sediments in Bernavis Area, Northern Iraq. Unpublished M.Sc Thesis, Baghdad University, p. 150B.